Forces on Particles Entrained in Turbulent Flow Through Rotating Channel

Krishnan V. Pagalthivarthi and **Pankaj K. Gupta**

Dept. of Applied Mechanics, Indian Institute of Technology, Hauz Khas, New Delhi 110016

Abstract: The problem of particulate flow in rotating channels serves as a useful benchmark for the more complex problem of solid-fluid mixtures in rotating passages. In a previous paper, the authors reported numerical simulation of the developing, two-dimensional (valid for large aspect ratio channels), steady (in the mean) and incompressible carrier-phase flow. This study quantifies the relative magnitudes of the most significant forces acting on a particle carried by a turbulent flow field in a rotating channel. Drag, pressure, Coriolis, centrifugal and virtual mass forces are considered. Particles are treated as uniform rigid spheres of specified diameter in determining the forces acting on them. During collision with the channel walls, they are treated as point masses. The variations of the forces on the particle along its particle trajectory are discussed.

Key words: *Entrained particles, rotating channel flow, forces acting on particles*

INTRODUCTION

Flow of dilute solid-fluid mixtures through rotating passages is important in slurry and pneumatic transportation of solids. Two important effects of the presence of solids in such applications are: (a) the additional head loss in the passages, and (b) erosion of wetted surfaces. Both of these factors have a strong bearing on the economics of the overall operation. It is, therefore, important to understand the behavior of entrained particles and the forces acting on them in rotating passages. The straight rotating channel provides a useful benchmark for developing robust numerical methods as well as for understanding the physics of particulate flow in such situations.

A number of studies [e.g., 1-6] deal with single-phase flow in rotating channels. In a recent paper [6], the authors reported the performance of an eddy viscosity model in predicting single-phase flow through two-dimensional channels rotating in orthogonal mode (the axis of rotation is normal to the plane of the channel). A number of studies have also been conducted [e.g., 7-10] on two-phase flow through stationary channels and pipes. However, studies involving two-phase flow through rotating channels are less common. Solid-liquid flow through rotating impellers has been addressed [11, 12] using inviscid flow assumption for the carrier phase. These studies do not report a quantitative assessment of the forces

acting on the particles. Moreover, viscous effects can significantly affect the base flow of the carrier, particularly near the walls.

There are few studies quantifying the relative magnitudes of the forces acting on particles entrained in flow through rotating channels. Such quantification can give valuable insight into the head loss and erosion phenomena. The aim of this study has been to quantify the forces on a typical particle in dilute solid-fluid flows through rotating channels.

Since the carrier-phase flow was dealt with in detail in a previous paper [6], the present study focuses mainly on the particles. Beginning with the equations of motion for a solid particle, a numerical method for tracking an individual particle is described. During collision with the walls, the particles are treated as point masses. Model coefficients of restitution are used in the normal and tangential directions to determine the particle velocity after impact. Impact is assumed to be instantaneous. The roughness of the channel walls generally have a statistical nature both in terms of the height of the surface irregularities as well as in terms of their direction with respect to the impacting particle. Some authors have attempted to include this randomness into their models for stationary passages with the concept of a virtual wall [13]. As a first approximation, this study assumes smooth walls, so that the direction of the normal to the wall is deterministic, not statistical. One-way coupling is assumed, *i.e.*, fluid flow affects the particulate flow, but not *vice versa*. Rotation is assumed to be in a horizontal plane, so that the effect of gravity may be neglected.

EQUATION OF MOTION AND NUMERICAL METHOD

In terms of the absolute coordinate system (*XYZ* in Figure 1.) the equation of motion of a typical particle is

$$\underbrace{\rho_S \forall \frac{d\vec{V}_p}{dt}}_{\text{Inertia}} = \underbrace{-\forall \nabla p}_{\text{Pressure}} + \underbrace{\frac{C_D A \rho}{2}\left|\vec{V}-\vec{V}_p\right|\left(\vec{V}-\vec{V}_p\right)}_{\text{Drag}} + \underbrace{\rho \forall C_v\left(\frac{d\vec{V}}{dt}-\frac{d\vec{V}_p}{dt}\right)}_{\text{Virtual Mass}}, \quad (1)$$

where ρ_S is the particle density; $\forall$ is the particle volume; t is the time; $\vec{V}_p$ and $\vec{V}$ are, respectively, the particle and fluid mean velocities with respect to ground; p is the fluid pressure; C_D is the drag coefficient; A is the project area, $\pi d_p^2/4$, of the particle of diameter d_p; ρ is the fluid density; $\hat{i}$ and $\hat{j}$ are the unit vectors in the *xyz* system. (coordinate system attached to rotating reference); and C_v (= 0.5 for spheres) is the virtual mass coefficient. The last term is negligible when $\rho << \rho_S$ (as in gas-solid systems).

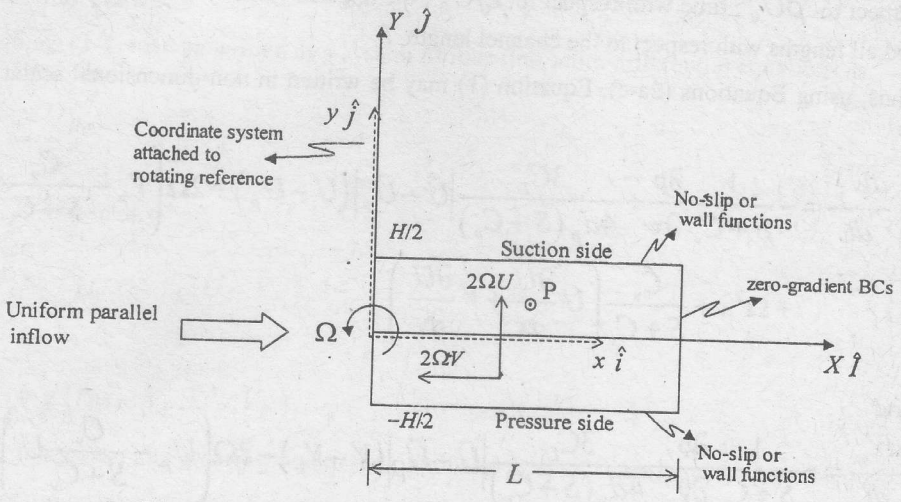

Figure 1. Particle entrained in rotating channel flow.

The relations between relative and absolute particle velocities and accelerations are

$$\vec{V}_p = \vec{U}_p + \vec{\Omega}\times\vec{r}, \text{ and } \frac{d\vec{V}_p}{dt} = \left(\frac{d\vec{U}_p}{dt}\right)_R + 2\vec{\Omega}\times\vec{U}_p + \vec{\Omega}\times\left(\vec{\Omega}\times\vec{r}\right), \quad \text{(2a, b)}$$

where $\vec{\Omega} = \Omega\hat{k}$ is the constant angular velocity of the channel. Similar expressions holdor the fluid velocity and acceleration. The subscript R denotes the rotating frame. The relative acceleration $\left(\frac{d\vec{U}}{dt}\right)_R$, the material derivative of velocity in the rotating frame, is given in terms of the local derivative and convective acceleration as

$$\left(\frac{d\vec{U}}{dt}\right)_R = \frac{\partial\vec{U}}{\partial t} + \left\{\left(\vec{U}\cdot\nabla\right)\vec{U}\right\}_R. \quad \text{(2c)}$$

Since the carrier mean flow is steady in the rotating frame of reference, $\frac{\partial\vec{U}}{\partial t} = 0$. For convenience, the subscript R is dropped, as there is no ambiguity in its meaning in what follows.

The equations are computer-coded most effectively in their non-dimensional form. Velocity is normalized with respect to the inlet uniform flow velocity, U_0; pressure with

respect to ρU_0^2; time with respect to L/U_0; the angular velocity with respect to U_0/L; and all lengths with respect to the channel length, L.

Thus, using Equations (2a-c), Equation (1) may be written in non-dimensional scalar form as

$$\frac{dU_p}{dt}=-\frac{1}{S+C_v}\frac{\partial p}{\partial x}+\frac{3C_D}{4d_p(S+C_v)}\left|\vec{U}-\vec{U}_p\right|\left(U-U_p\right)+2\Omega\left(V_p-\frac{C_v}{S+C_v}V\right)$$
$$+\Omega^2 x+\frac{C_v}{S+C_v}\left(U\frac{\partial U}{\partial x}+V\frac{\partial U}{\partial y}\right) \tag{3}$$

and

$$\frac{dV_p}{dt}=-\frac{1}{S+C_v}\frac{\partial p}{\partial y}+\frac{3C_D}{4d_p(S+C_v)}\left|\vec{U}-\vec{U}_p\right|\left(V-V_p\right)-2\Omega\left(U_p-\frac{C_v}{S+C_v}U\right)$$
$$+\Omega^2 y+\frac{C_v}{S+C_v}\left(U\frac{\partial V}{\partial x}+V\frac{\partial V}{\partial y}\right), \tag{4}$$

where S is the relative density of the solid, and U_p and V_p (U and V) are the scalar components of the relative velocity of the particle (fluid).

The drag coefficient, C_D, is calculated from the empirical correlation [12],

$$C_D=\begin{cases}0.44 & \text{when } Re_p>1000\\ \left(24/Re_p\right)\left(1+0.14Re_p^{0.7}\right) & \text{when } Re_p\le 1000,\end{cases} \tag{5}$$

where the particle Reynolds number, Re_p, is defined as

$$Re_p=\frac{\left|\vec{U}-\vec{U}_p\right|d_p}{\upsilon}. \tag{6}$$

For certain combinations of operating parameters, (Re_H, Ro_H, ρ/ρ_s *etc.*), the particles may slide along the channel wall. In such a case, the particle experiences a kinetic frictional resistance $\mu_k F_n$, where F_n is the y-component (normal to the wall) of all the forces acting on the particle due to drag, pressure, Coriolis, centrifugal and virtual mass forces. If the effective normal force is directed away from the wall, the particle is about to separate from the substrate, and then the friction force is zero.

A fourth order Runge-Kutta method [14] is employed to integrate the initial value problem represented by Equations (3) and (4). The initial position and velocity of the particle are

specified at channel entry. The initial particle velocity is taken as equal to that of the carrier fluid at inlet.

Equations (3-4) may be written as a system of four first order differential equations as

$$\frac{dx_P}{dt} = U_P, \tag{7a}$$

$$\frac{dy_P}{dt} = V_P, \tag{7b}$$

$$\frac{dU_P}{dt} = f\left(t, x_P, y_P, U_P, V_P\right), \tag{7c}$$

and

$$\frac{dV_P}{dt} = g\left(t, x_P, y_P, U_P, V_P\right), \tag{7d}$$

where functions f and g correspond to the right hand sides of Equations (3-4), respectively.

For notational convenience, Equations (7a-d) may be written in vector form as

$$\underset{\sim}{W} = \underset{\sim}{q}\left(t, \underset{\sim}{W}\right), \tag{8a}$$

where

$$\underset{\sim}{W} = \left(x_P, y_P, U_P, V_P\right)^T, \tag{8b}$$

and

$$\underset{\sim}{q} = \left(U_P, V_P, f, g\right)^T. \tag{8c}$$

The prescribed initial condition is $\underset{\sim}{W}(0) = \underset{\sim}{W}_0$. The fourth order Runge-Kutta method in this study uses the following marching procedure:

$$\underset{\sim}{W}(t+\delta t) = \underset{\sim}{W}(t) + \frac{\delta t}{6}\left(k_1 + 2k_2 + 2k_3 + k_4\right) + O(\delta t)^5, \tag{9}$$

where

$$\underset{\sim}{k}_1 = \underset{\sim}{q}\left(t, \underset{\sim}{W}(t)\right), \tag{10a}$$

$$\underset{\sim}{k}_2 = \underset{\sim}{q}\left(t + \frac{\delta t}{2}, \underset{\sim}{W}(t) + \frac{\underset{\sim}{k}_1 \delta t}{2}\right), \tag{10b}$$

$$\underset{\sim}{k}_3 = \underset{\sim}{q}\left(t + \frac{\delta t}{2}, \underset{\sim}{W}(t) + \frac{\underset{\sim}{k}_2 \delta t}{2}\right), \tag{10c}$$

and

$$\underset{\sim}{k}_4 = \underset{\sim}{q}\left(t + \delta t, \underset{\sim}{W}(t) + \underset{\sim}{k}_3 \delta t\right), \tag{10d}$$

where δt is the local time step.

Special treatment is necessary for handling particle collisions with the channel walls. Particles are treated as spheres of definite diameter while solving Equations (3) and (4). When determining the position of the particle at impact with the walls, the particles are treated as material points. In the present study, particle-wall collisions are treated as instantaneous. A coefficient of restitution is introduced in both the tangential and the normal directions to compute the post-impact velocity of the particle. The channel is assumed to be unaffected in the rotating reference frame by the collisions.

In Figure 2, let U_{P1}, V_{P1} and U_{P2}, V_{P2} be the initial and final velocities of the particle during a time step δt. Let $\mathrm{A}(x_1, y_1)$ and $\mathrm{B}(x_2, y_2)$ be the corresponding two positions of the particle. In the absence of the wall, the particle would trace out the path represented by the solid curve AB. The presence of the wall implies that the particle will collide before reaching point B.

The point of impact $\mathrm{C}(x_s, y_s)$ may be determined by iteration. However, if the time step is small enough, a simple interpolation gives an accurate enough prediction of the point C and the particle velocity at the point of impact. Linear interpolation is used between A and B to locate the point C of impact. The actual time δt_1 from A to C is also computed by interpolation.

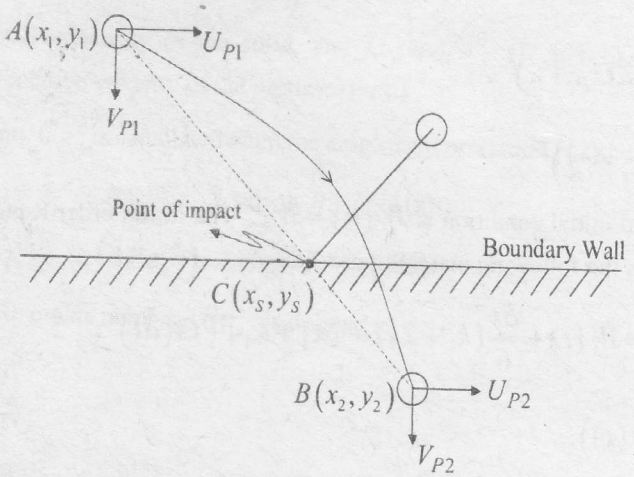

Figure 2. Interpolation to determine point of impact.

Two more practical points are worth mentioning. First, it is possible that the post-impact normal velocity component may be quite small. In such a case, below a cut-off value, the y-component of the velocity at the wall may be set to zero, so that the particle just slides along the channel wall. Second, the center of the spherical particle can never touch the wall. In computing particle trajectory, the particle is assumed to be a material point. Thus, the wall is hypothetically shifted to the particle center, without introducing significant error. This procedure is acceptable, if the particle size is much smaller than the characteristic dimensions of the channel.

DISCUSSION OF RESULTS

The testing and validation of code by mesh refinement and comparison with published results for a stationary channel are discussed elsewhere [6, 15]. In this section, the variations of the drag, pressure, Coriolis and centrifugal forces acting on the particle (as it moves along its trajectory in air and water) are presented.

In the figures of this section, all quantities are non-dimensionalized, unless otherwise stated. For clarity, only the particle released at $y=0$ (mid-height of the channel) is considered. All calculations are for the operating parameters shown in Table 1. In non-dimensional terms, the inlet velocity of both the fluid and the particle is unity.

In Table 1, the quantities d_p^* and v_{ts}^* are the non-dimensional settling velocity of the particle in a rotating environment. These definitions are analogous to similar quantities defined for settling under the action of gravity [16]. For the rotating environment, these are defined as

$$d_p^* = d_p \left[\frac{\rho(\rho_p - \rho)(2\Omega U_0)}{\mu^2} \right]^{\frac{1}{3}} \tag{11}$$

and

$$v_{ts}^* = 1.73 \sqrt{g d_p \left(\frac{\rho_p}{\rho} - 1 \right)} \left[\frac{\rho^2}{\mu(\rho_s - \rho)(2\Omega U_0)} \right]^{\frac{1}{3}}. \tag{12}$$

It is clear from Table 1 that for the same physical diameter of $d_p = 1$ mm, the corresponding non-dimensional diameter in water is much smaller than that in air. Similarly the non-dimensional settling velocity is much larger for air than for water as the carrier. These quantities, as will be seen, characterize particle behavior to a large extent.

Table 1. Details of operating parameters

Case	Re_H	Ro_H	ρ_p $(\mathrm{kg/m^3})$	ρ $(\mathrm{kg/m^3})$	d_p (mm)	e_x	e_y	μ_k	d_p^*	v_{ts}^*
1.	11500	0.21	2700	1.23	1	1	1	0.1	99.15	17.23
2.	11500	0.21	2700	1000	1	1	1	0.1	9.105	5.22
3.	11500	0.21	1000	1.23	1	1	1	0.1	71.18	14.60

In the figures, the ordinate axis on the left-hand side of each figure shows the y-coordinate of the particle trajectory. The two ordinate axes on the right-hand side of each figure show, respectively, the x-component and y-component of force (or velocity). Before getting an insight into the forces on the particle, it is useful to get an idea of the velocity variation.

Variation of Velocity of Particle

The variation of particle velocity along the length of the channel is shown in Figures 3a and 3b for air and water, respectively, as the carrier phases. The calculations correspond to Cases 1 and 2 of Table 1.

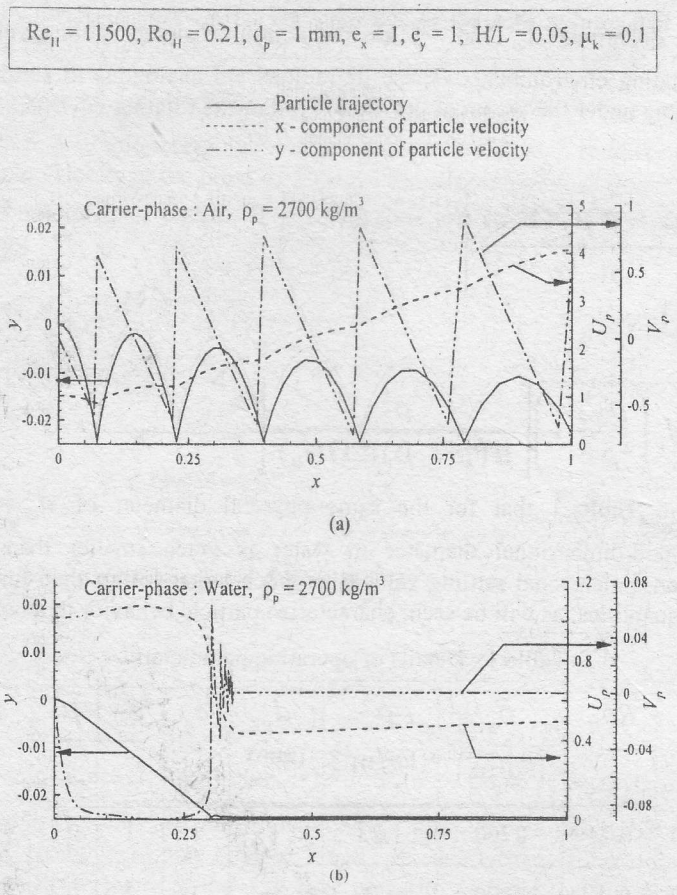

Figure 3. Variation of particle velocity for Cases 1 and 2 of Table 1 with carrier-phase as (a) air, and (b) water.

The x-component of particle velocity, U_p, increases (Figure 3a) as the particle moves along the channel length. The y-component of particle velocity, V_p, shows discontinuity at the positions of impact because V_p changes sign at points of impact. The increase in U_p is due to the centrifugal force, which varies as $\Omega^2 x$. By intuition, we would expect the drag force to decrease V_p as the particle moves towards the exit. However, for air (Figure 3a), a slight increase in V_p is seen as x increases. This corresponds to the increase in U_p and hence in the Coriolis force, which varies as $2\Omega U_p$. In the absence of drag force, the increase in V_p would be greater than that indicated by Figure 3a.

For water as the carrier, the variation of particle velocity, shown in Figure 3b, is seen to be completely different from that for air (Figure 3a). The drag effect in case of water is much more significant than in case of air. In Figure 3b, U_p increases initially up to $x \approx 0.125$. At this stage, drag catches up and slows down the particle till it impacts with the channel pressure-side wall. After a few feeble bounces, the particle begins to slide along under the combined influence of drag and Coriolis forces. The discontinuous oscillations in V_p indicate the feeble bounces before sliding begins. After sliding begins, the centrifugal force gradually overpowers friction and drag, so that the particle begins to slowly speed up again. As the particle moves towards the pressure side, it accelerates (V_p increases) under the influence of Coriolis force. At impact, V_p reverses sign and then decelerates (since Coriolis force is now opposite to V_p).

When the particle is neutrally buoyant ($\rho_p = \rho = 1000\ \mathrm{kg/m^3}$), Figure 4 indicates that the particle essentially moves parallel to the channel walls, following the carrier flow. In this case, V_p is nearly zero everywhere, and U_p increases and reaches a plateau as the centerline velocity of the carrier fluid increases and reaches its fully developed value.

Variation of Pressure Force

In Figures 5a and 5b, the variations of the x- and y- components of pressure force are shown for air and water, respectively. Note from Equations (3-4) that the pressure force contains $-\nabla p$ (the negative of pressure gradient). From Figures 6a, for a specified y, the pressure is seen to increase with x. The pressure gradient $\dfrac{\partial p}{\partial x}$ continues to increase with x and so does the magnitude of pressure force on the particle. Theoretically, the pressure gradient in

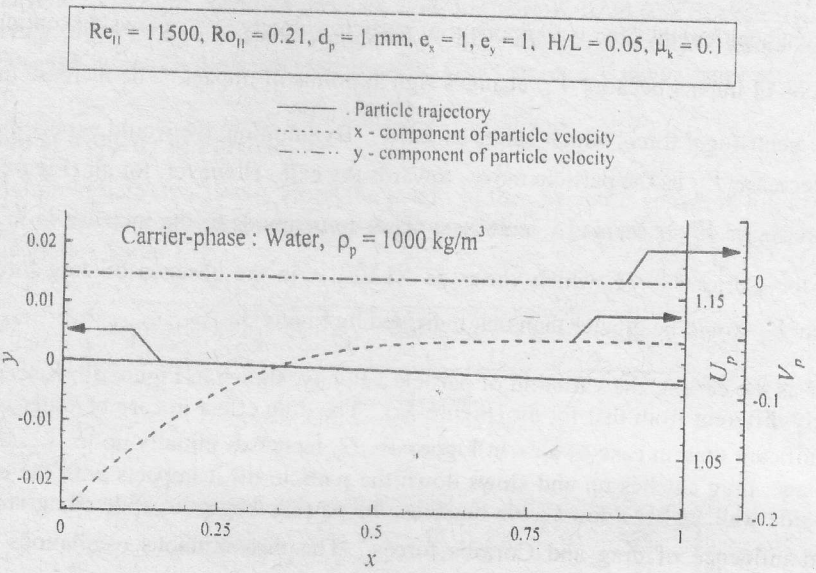

Figure 4. Variation of particle velocity for neutrally buoyant particle (ρ_p = 1000kg/m^3) with water as carrier-phase.

x-direction should vary as $\Omega^2 x$ (Figure 6a). This is reflected as a linear increase in the magnitude of the pressure force, pf_x, in Figures 5a and 5b.

The pressure force, pf_y, in the y-direction varies in a somewhat complex manner. Right at and in the vicinity of the pressure-side wall, the pressure gradient ($2\Omega U$) is nearly zero because of no-slip. Away from the wall, pressure varies linearly with y as shown in Figure 6b, *i.e.*, the pressure gradient, $\frac{\partial p}{\partial y}$ is a negative constant away from the wall. Thus, for a particle released at $y = 0$, as the particle moves towards the channel base (pressure side), initially, the pressure force pf_y, is roughly constant. As the particle approaches the wall, the *magnitude* of pressure gradient suddenly drops, and so does the pressure force. After the particle impacts and moves away from the base, the pressure force again rises suddenly. In case of air (Figure 5a), the particle reaches a substantial peak into the mainstream of the flow, *i.e.*, it reaches the constant pressure force zone after impact. Thus, pf_y remains nearly constant for some part of the trajectory, and again the process is repeated along the particle trajectory.

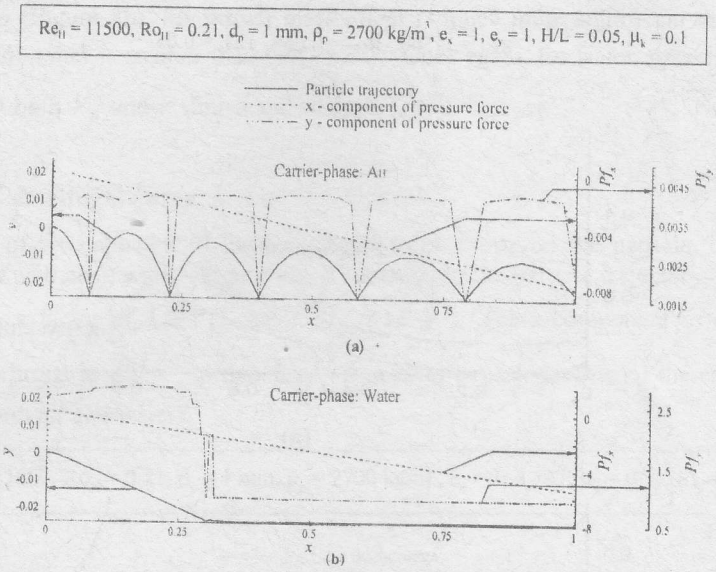

Figure 5. Variation of pressure force acting on the particle with carrier-phase as (a) air, and (b) water.

In the case of water (Figure 5b), the particle does not move sufficiently far from the wall after the bounce. Thus, pf_y does not quite increase as much as in the case of air. Once the particle starts sliding, pf_y also attains a constant value.

Variation of Drag Force

Variations for drag forces, Df_x and Df_y are shown in Figures 7a and 7b, respectively, for air and water. As noted with reference to Figure 3a, U_p tends to increase with x. Thus, the slip velocity $(U_p - U)$ increases and so does the particle Reynolds number. The drag force, which is proportional to $(U - U_p)$ (Equation 3), increases in magnitude (note the negative sign). Discontinuous sign reversals are seen in Df_y corresponding to the impact locations, where V_p changes sign. Furthermore, as the particle traverses along its trajectory, V_p decreases in magnitude, which results in a decrease in $|V_p - V|$, and hence a decrease in Re_p with increasing x. Thus in an overall sense $|Df_y|$ increases with x. For the case of water, Figure 7b, the particle begins to slide for $x >$ 0.3 and the drag force $|Df_y|$ is zero. Note that the magnitude of drag force in air is much smaller than that in water.

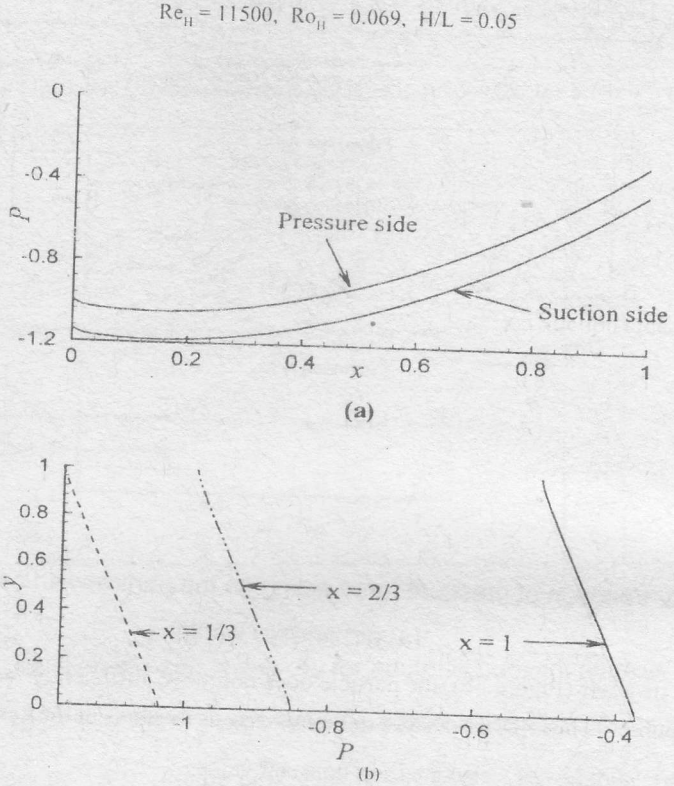

Figure 6. Variation of pressure (a) along the channel length, and (b) across the channel height.

Variation of Coriolis Force

The variation of Coriolis force acting on the particles in airflow is shown in Figure 8a. Including the effect of virtual mass, the non-dimensionalized x-component of Coriolis force is, $2\Omega\left(V_p - \frac{C_v}{S+C_v}V\right)$ and its y-component is $-2\Omega\left(U_p - \frac{C_v}{S+C_v}U\right)$. The discontinuities in Cof_x at the points of impact match with those in V_p. The y-component of Coriolis force increases in magnitude along the channel length because the term, $+2\Omega\left(U_p - \frac{C_v}{S+C_v}U\right)$, increases along the channel length.

For water flow (Figure 8b), the virtual mass effect is much more significant than for air. Thus, Cof_y for water is smaller than that for air. Once again, for water, once the particle begins to slide, both V_p and V vanish and so does Cof_x.

Variation of Centrifugal Force

The variation of y-component of the centrifugal force acting on the particle, both in air (Figure 9a), as well as in water (Figure 9b) is identical to the particle trajectory except that it is scaled by a factor of Ω^2. (Note: $Cef_y = \Omega^2 y$.) The x-component of centrifugal force is proportional to $\Omega^2 x$, so that Cef_x is seen to be independent of the carrier (it is identical for both air and water).

$Re_H = 11500$, $Ro_H = 0.21$, $d_p = 1$ mm, $\rho_p = 2700$ kg/m^3, $e_x = 1$, $e_y = 1$, $\mu_k = 0.1$, $H/L = 0.05$

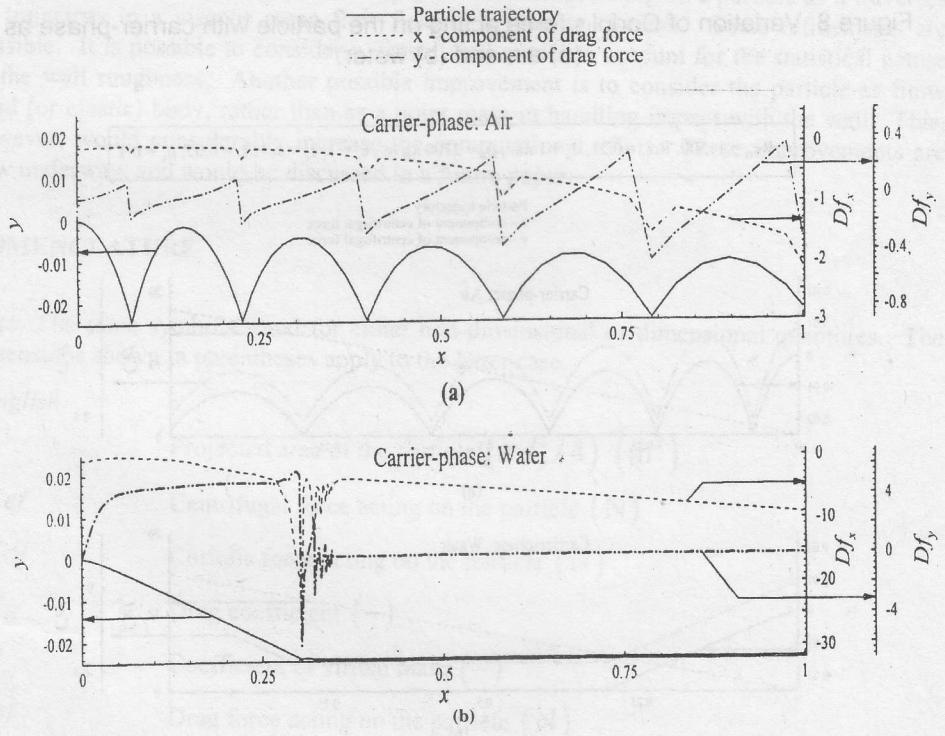

Figure 7. Variation of drag force acting on the particle with carrier-phase as (a) air, and (b) water.

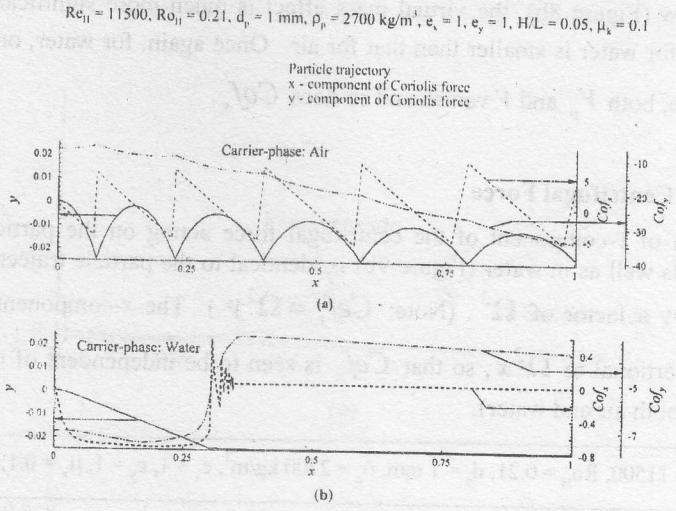

Figure 8. Variation of Coriolis force acting on the particle with carrier-phase as (a) air, and (b) water.

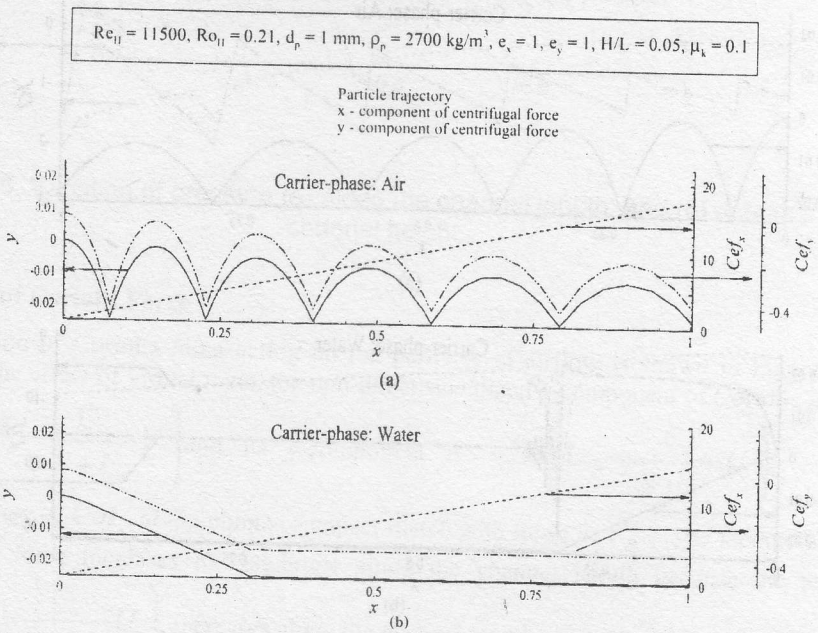

Figure 9. Variation of centrifugal force acting on the particle with carrier-phase as (a) air, and (b) water.

In summary, it is seen that the Coriolis, drag and centrifugal forces on the particle are predominant in air. In particular, the Coriolis force greatly determines the particle trajectory. In water, pressure forces are also comparable to the other forces. From the trajectories, it is that with water as the carrier, the particles tend to slide along the channel, with hardly a few feeble bounces. In addition, since the Coriolis force on the particle increases with x, the sliding wear rate along the pressure side of the channel may be expected to increase with x. This is actually observed in the Coriolis wear tester [17]. In sharp contrast, with air as the carrier, hardly any sliding is seen. Thus, the wear mechanism in the case of air is likely to be governed by particle impact. In practice, the standard Coriolis wear tester may be modified for pneumatic tests with particles in order to measure impact wear coefficients.

CONCLUDING REMARKS

The paper presents a quantitative description of the forces acting on a particle as it traverses its trajectory in a viscous mean flow field in a rotating channel. Some refinements are possible. It is possible to consider a virtual wall model to account for the statistical nature of the wall roughness. Another possible improvement is to consider the particle as finite rigid (or elastic) body, rather than as a point mass in handling impact with the wall. This, however, would considerably increase the computational effort. These improvements are now underway, and would be discussed in a future paper.

NOMENCLATURE

Note: The same symbols stand for either non-dimensional or dimensional quantities. The dimensions shown in parentheses apply to the latter case.

English

A	Projected area of the particle $\left(\pi d_p^2/4\right)$ $\left(\mathrm{m}^2\right)$
Cef	Centrifugal force acting on the particle $\left(\mathrm{N}\right)$
Cof	Coriolis force acting on the particle $\left(\mathrm{N}\right)$
C_D	Drag coefficient $\left(-\right)$
C_v	Coefficient of virtual mass $\left(-\right)$
Df	Drag force acting on the particle $\left(\mathrm{N}\right)$
d_p	Particle diameter $\left(\mathrm{m}\right)$
d_p^*	Non-dimensional particle diameter (see Eq. 11) $\left(-\right)$

F_n	y-component of all the forces acting on the particle (N)
g	Acceleration due to gravity $(\mathrm{m/s^2})$
H	Height of the channel (m)
$\hat{I},\hat{J},\hat{K}$	Unit vectors in X-, Y- and Z- directions respectively
$\hat{i},\hat{j},\hat{k}$	Unit vectors in x-, y- and z- directions respectively
$\underset{\sim}{k}_1,\underset{\sim}{k}_2,\underset{\sim}{k}_3,\underset{\sim}{k}_4$	Vectors computed during Runge-Kutta steps
L	Length of the channel (m)
O	Of the order of
p	Pressure $(\mathrm{N/m^2})$
pf	Pressure force acting on the particle (N)
$\underset{\sim}{q}$	Vector defined in Equation (8c)
Re	Length based Reynolds number $(-)$
Re_H	Height based Reynolds number $(-)$
Re_p	Particle Reynolds number $(-)$
Ro	Rotation number $(-)$
Ro_H	Height based rotation number $(-)$
Ro_x	Rotation number based on distance x from origin $(-)$
$\vec{r}$	Position vector (m)
S	Ratio of solid density to fluid density (Eqs. 3 and 4) $(-)$
t	Time (m)
U	x-component of $\vec{U}$ $(\mathrm{m/s})$
$\vec{U}$	Fluid mean velocity vector with respect to rotating reference $(\mathrm{m/s})$
U_p	x-component of $\vec{U}_P$ $(\mathrm{m/s})$
U_p	x-component of particle velocity $(\mathrm{m/s})$
$\vec{U}_p$	Particle mean velocity vector with respect to rotating reference $(\mathrm{m/s})$
U_0	Inlet velocity $(\mathrm{m/s})$

V	y-component of $\vec{U}$ $(\mathrm{m/s})$
$\vec{V}$	Fluid mean velocity vector with respect to inertial reference $(\mathrm{m/s})$
$\vec{V}_p$	Particle mean velocity vector with respect to inertial reference $(\mathrm{m/s})$
V_p	y-component of $\vec{U}_p$ $(\mathrm{m/s})$
V_p	y-component of particle velocity $(\mathrm{m/s})$
v_{ts}^*	Non-dimensional terminal velocity of the particle $(-)$
$\underset{\sim}{W}$	Vector of particle position and velocity defined in Equation (8b)
XYZ	Coordinate system attached to inertial reference frame
xyz	Coordinate system attached to rotating reference frame

Greek

δt	Time step in Runge-Kutta integration (s)
μ_k	Coefficient of kinetic friction $(-)$
μ	Laminar viscosity $(\mathrm{kg/m \cdot s})$
ρ	Fluid density $(\mathrm{kg/m^3})$
ρ_P or ρ_s	Particle (solid) density $(\mathrm{kg/m^3})$
υ	Laminar kinematic viscosity $(\mathrm{kg/m \cdot s})$
Ω	Angular speed $(\mathrm{rad/s})$
$\vec{\Omega}$	Angular velocity vector $(\mathrm{rad/s})$
$\forall$	Particle volume $(\mathrm{m^3})$
∇	Gradient operator

Subscripts

i, j, k	Dummy indices
P	Quantities pertaining to a particle
R	Relative
x	component in direction of x-axis
y	component in direction of y-axis

ACKNOWLEDGEMENTS

The authors are thankful to Vipin Narang for his help in preparing the manuscript.

REFERENCES

[1] Howard J.H.G., Patankar S.V. and Bordynuik R.M., 1980, "Flow Prediction in Rotating Ducts Using Coriolis-Modified Turbulence Models," *ASME J. Fluids Eng*, Vol. 102, pp. 456-461.

[2] Younis B.A., 1993, "Prediction of Turbulent Flows in Rotating Rectangular Ducts," *Transactions of the ASME FED*, Vol. 115, pp. 646-652.

[3] Johnston J.P., Halleen R.M. and Lezius D.K., 1972, "Effects of Spanwise Rotation on the Structure of Two-Dimensional Fully Developed Turbulent Channel Flow, " *J Fluid Mech.*, Vol. 56, pp. 533-557.

[4] Pagalthivarthi K.V. and Ramanathan V.R., 2001, "Finite Element Prediction of Viscous Free Surface Flow in Rotating Channel," *Int. J. Num. Meth. Fluids*, Accepted for Publication (MS#G00-31).

[5] Majumdar A.K. and Spalding D.B., 1977, "Numerical Investigation of Three-Dimensional Flows in a Rotating Duct by a Partially Parabolic Procedure," *ASME Paper* 77-WAFE-7.

[6] Pagalthivarthi K.V. and Gupta P.K., 2001, "Performance of Eddy Viscosity Model in Rotating Channel Flow," *J. Mech. Eng. Res. Dev.*, (communicated).

[7] Tsuji Y., Morikawa Y., Tanaka T., Nakatsukasa N. and Nakatani M., 1987, "Numerical Simulation of Gas-Solid Two-Phase Flow in a Two-Dimensional Horizontal Channel," *Int. J. Multiphase Flow*, Vol. 13, pp. 671-684.

[8] Nguyen A.V. and Fletcher C.A.J., 1999, "Particle Interaction with the Wall Surface in Two-Phase Gas-Solid Particle Flow," *Int. J. Multiphase Flow*, Vol. 25, pp. 139-154.

[9] Roco M.C. and Shook C.A., 1983, "Modeling of Slurry Flow: The Effect of Particle Size," *Canadian Journal of Chemical Engineering*, Vol. 61, pp. 494-503.

[10] Roco M.C. and Shook C.A., 1991, "Slurry Flow Principles," Butterworth-Heinemann Series in Chemical Engineering.

[11] Roco M.C. and Reinhardt E., 1980, "Calculation of Solid Particle Concentration in Centrifugal Impellers Using Finite Element Technique," *Proc. Hydrotransport 7 Conf., BHRA*, pp. 359-376.

[12] K. Minemura, T. Uchiyama, Calculation of the three-dimensional behavior of spherical solid particles entrained in a radial-flow impeller pump, *Proc. Instn. Mech. Engrs. Part C: Journal of Mechanical Engineering Science* 204 (1990) 159-168.

[13] Sommerfeld M., 1992, "Modeling of Particle-Wall Collisions in Confined Gas-Particle Flows," *Int. J. Multiphase Flow*, Vol. 18, pp. 905-926.

[14] Carnahan B., Luther H. A. and Wilkes J. O., 1969, "Applied Numerical Methods," John Wiley and Sons, New York.

[15] Carnahan B., Luther H. A. and Wilkes J. O., 1969, "Applied Numerical Methods," John Wiley and Sons, New York.

[16] Wilson K. C., Addie G. R. and Clift R., 1992, "Slurry Transport Using Centrifugal Pumps," Elsevier Science Publishers Ltd., Essex, England.

[17] Tuzson J. J. and Clarke H. Mcl., 1998, "Slurry Erosion Process in the Coriolis Wear Tester," *ASME-FED*, Paper No. FEDSM98-5144.